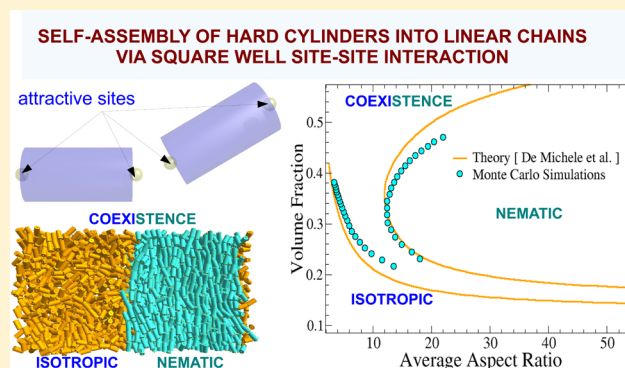


## Self-Assembly-Driven Nematization

Khanh Thuy Nguyen,<sup>†</sup> Francesco Sciortino,<sup>†,‡</sup> and Cristiano De Michele\*<sup>†</sup><sup>†</sup>Dipartimento di Fisica, and <sup>‡</sup>Istituto dei Sistemi Complessi (ISC)–Consiglio Nazionale delle Ricerche (CNR), “Sapienza” Università di Roma, Piazzale Aldo Moro 5, 00185 Rome, Italy

## Supporting Information

**ABSTRACT:** The anisotropy of attractive interactions between particles can favor, through a self-assembly process, the formation of linear semi-flexible chains. In the appropriate temperatures and concentration ranges, the growing aspect ratio of the aggregates can induce formation of a nematic phase, as recently experimentally observed in several biologically relevant systems. We present here a numerical study of the isotropic–nematic phase boundary for a model of bifunctional polymerizing hard cylinders, to provide an accurate benchmark for recent theoretical approaches and to assess their ability to capture the coupling between self-assembly and orientational ordering. The comparison indicates the importance of properly modeling excluded volume and orientational entropy and provides a quantitative confirmation of some theoretical predictions.



## INTRODUCTION

Self-assembly is the process of reversible aggregation of basic building blocks. Aggregating monomers can be simple molecules, macromolecules, or colloidal particles; i.e., their size can range from a few angstroms to micrometers. Self-assembly is thus of paramount interest in material science, soft matter, and biophysics.<sup>1–3</sup>

The simplest but nonetheless relevant self-assembly process takes place when attractive interactions between the building blocks lead to the formation of linear aggregates. Micellar systems,<sup>4–6</sup> fibers and fibrils,<sup>7–10</sup> aqueous solutions of short (nano)<sup>11,12</sup> and long B-DNA,<sup>13–16</sup> G-quadruplexes,<sup>17</sup> chromonics,<sup>18–22</sup> and colloidal polymers<sup>23</sup> are all examples of systems where anisotropic attractive interactions between the aggregating units induce the formation of an isotropic phase of (exponentially polydisperse in length) semi-flexible reversible chains. Such an aggregation process, at small monomer concentration, is well-understood.<sup>5,24,25</sup> More complex is the description of the collective behavior of these systems when the monomer concentration increases. It has been experimentally observed that, above a critical concentration, the mutual alignment of the assembled chains gives rise to the formation of macroscopically orientationally ordered liquid crystal phases.<sup>7,11,26,27</sup> Indeed, even in the case in which the residual interaction between chains is only excluded volume, the assembly process results in an increase of the average aggregate aspect ratio. In agreement with predictions of the venerable Onsager theory,<sup>28</sup> orientational ordering (nematic transition) becomes inevitable if chains are sufficiently rigid. Despite the relevance of the phenomenon, accurate modeling of the isotropic–nematic transition in the presence of equilibrium

polymerization is still an open problem. Several theoretical approaches<sup>5,29–32</sup> in the last few years have attempted to tackle the problem, modeling in different ways the excluded volume interactions and the entropic contribution associated with chain flexibility.

These studies have clarified the importance of the particle shape and polydispersity induced by the self-assembly process in controlling the transition and the different orientational properties of short chains, which might also retain isotropy in the nematic phase. Unfortunately, no accurate estimates of the isotropic–nematic boundary for a simple and well-defined model undergoing equilibrium polymerization that could be used to assess the theoretical predictions are available in the literature. It is indeed rather difficult to precisely locate the isotropic–nematic transition, even in one-component (non-polymerizing) systems.<sup>33–43</sup>

To assess the validity of theoretical predictions, it is advisable to employ a simple model for which the phase diagram (and other quantities of interest) can be calculated with high accuracy via computer simulations. In addition, theoretical approaches require an accurate estimate of some input parameters for a given model (or real system). These parameters can be calculated accurately only for simple models. We thus opted for a system of polymerizing hard cylinders (HCs) with aspect ratio  $X_0 = L/D = 2.0$ , where  $L$  is its length and  $D$  is its diameter, for which we report in this paper an exhaustive numerical study. The value  $X_0 = 2.0$  ensures that, in

Received: January 10, 2014

Revised: February 27, 2014

Published: April 4, 2014

the absence of polymerization, monomers cannot form a nematic phase.<sup>33</sup> Thus, self-assembly is the only mechanism that can induce orientational ordering. The two cylinder bases are decorated with two square-well (SW) sites, responsible for the reversible polymerization process. We observe a nematic phase at low temperatures  $T$  and accurately evaluate the volume fraction of the coexisting isotropic and nematic phases for several  $T$ .

We find that, while the average chain length along the isotropic boundary increases progressively with cooling, the average chain length along the nematic boundary has a minimum at intermediate  $T$ . This re-entrant behavior is peculiar of self-assembly-driven nematization. Recent theoretical parameter-free calculations for the quasi-HC model<sup>32</sup> had indeed suggested such a re-entrance, but numerical or experimental evidence has not yet been observed. Our results thus provide not only a benchmark for future theoretical investigations but also a first quantitative assessment of a recent theoretical study.<sup>32,44</sup>

## MODEL

We investigate a simple model consisting of HCs of length  $L$  and diameter  $D$ , which are decorated with two attractive sites on their bases (Figure 1).

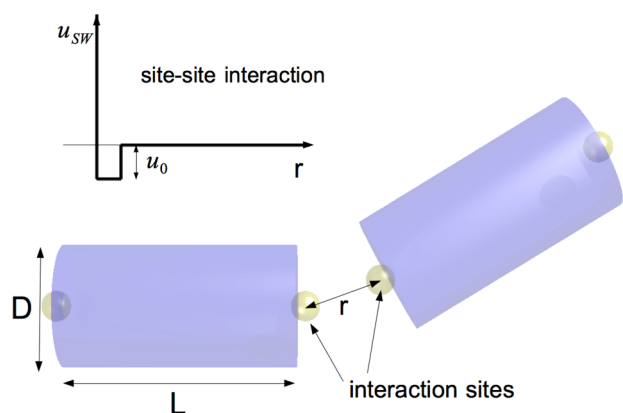


**Figure 1.** Investigated HC model. The centers of the two small yellow spheres indicate the sites interacting via the SW potential (shown on the top). The diameter of yellow spheres indicates the interaction range, i.e., the width of the well.  $u_0$  is the depth of the well, i.e., the binding energy. The cylinder diameter is  $D$ , and its length is  $L$ .

These two attractive sites are located along the symmetry axis (see Figure 1) at a distance  $L/2 + 0.15D/2$  from the HC center of mass, and sites belonging to distinct particles interact via the SW potential, i.e.,  $\beta u_{SW} = -\beta u_0$ , if  $r < \delta$ , and  $\beta u_{SW} = 0$ , if  $r > \delta$ , where  $r$  is the distance between the interacting sites,  $\delta = 0.25D$  is the interaction range (i.e., the diameter of the attractive sites), and  $\beta u_0$  is the ratio between the binding energy and the thermal energy  $k_B T$ , where  $k_B$  is the Boltzmann constant. In the following, we will make use of the adimensional temperature  $T^* = k_B T / u_0$ . Here,  $u_0$  does not depend upon the aggregate size; i.e., the self-assembly process is assumed to be isodesmic.<sup>45,46</sup>

The patch geometry ensures that no branching can occur in the system. In addition, the position and diameter of the patches have been chosen to generate a persistent length and a bonding volume compatible with values recently used in the analysis of DNA duplexes self-assembly, which can be found in ref 32.

## NUMERICAL METHODS

We implement the Kofke thermodynamic integration (KI) over temperature<sup>47–49</sup> to estimate the isotropic–nematic phase boundary.

KI consists of integrating numerically the Clausius–Clapeyron equation, i.e.

$$\left( \frac{d \ln P}{d\beta} \right)_{\text{coex}} = - \frac{\Delta h}{\beta P \Delta v} \quad (1)$$

where  $P$  is the pressure of the system,  $\Delta h$  is the enthalpy per particle difference between the two phases, and  $\Delta v$  is their volume per particle difference. At each integration step,  $h$  and  $v$  are computed by separate Monte Carlo (MC) isothermal–isobaric (NPT) simulations for the two coexisting phases. The isobaric MC simulations, which are used in the KI, employed the cluster NPT algorithm proposed in ref 50. For these simulations, we used  $N = 1000$  particles and performed two integrations over temperature starting from  $T^* = 0.149$  up to 0.195 and down to 0.12. Further details are provided in the Supporting Information.

The KI method requires a starting point located on the coexistence line. We evaluate such a point by successive umbrella sampling (SUS) MC simulations<sup>51,52</sup> carried out at  $T^* = 0.149$ . In this method, the probability  $P(N)$  of finding  $N$  particles at a fixed volume, temperature, and chemical potential [i.e., in the grand canonical (GC) ensemble] is computed and analyzed to evaluate coexistence between different phases.<sup>51,52</sup> SUS is a method to efficiently calculate  $P(N)$  (exploiting the availability of multiple processor clusters) by partitioning the investigated range of particles in several overlapping regions and performing (in parallel) independent GC–MC simulations in each of them. Matching  $P(N)$  in the overlapping parts allows one to rebuild the entire distribution. The coexistence chemical potential is estimated through a standard histogram reweighting technique (see Supporting Information for details), enforcing an equal-area condition below the  $P(N)$  peaks associated with the isotropic and nematic coexisting phases.

The box shape in SUS simulations is not cubic, as suggested by ref 52. Specifically, we use  $L_x = 13L$ ,  $L_y = 4L$ , and  $L_z = 23.5L$ , where the  $x$  axis is the nematic director, to have an interface that builds parallel to the  $xy$  plane (see Figure 2b). In the SUS starting configuration, all particles are aligned along the  $x$  axis. With this choice, chains of up to 13 particles in the nematic phase do not span the box, reducing any possible finite size effect. We have checked that aggregates longer than  $13L$ , when present, do not percolate, because of the chain flexibility. Three SUS simulations at  $T^* = 0.12$ , 0.135, and 0.158 were performed as checkpoints for the KI.

In addition, we performed canonical NVT MC simulations starting from the volume fractions obtained from KI to provide an accurate estimate of average energies at coexistence. In NPT and NVT MC simulations, we used a cubic box for the isotropic phase with  $L_x = L_y = L_z \approx 4L$  and an elongated box for the nematic phase with  $L_x = L_y \approx 5L$  and  $L_z \approx 20L$  ( $z$  axis is parallel to the nematic director). In all simulations, we employed periodic boundary conditions in all directions.

As extensively discussed in ref 30, the structure of the nematic phase is governed by the deflection length  $\lambda/L \approx (1 - S)l_p/3$ , where  $S$  is the nematic order parameter and  $l_p$  is the persistence length in units of monomers. In the present model,  $l_p \approx 11.6$  (see section 3.1 of the Supporting Information). According to the data reported later, an overestimate for the nematic order parameter in the nematic phase is  $S \geq 0.4$ . Hence,  $\lambda \leq 2.3L$ . Because in our simulations  $L_z \gg 2.3L$ , finite size effects are not expected to be significant. As a further test, we checked that chains did not percolate in any direction.

## RESULTS AND DISCUSSION

The probability distribution  $P(N)$  of observing at coexistence  $N$  particles in the simulation box at fixed  $T$  and chemical potential is shown in Figure 2b for two different  $T$ . The chemical potential at coexistence is determined via standard histogram reweighting techniques, imposing equal area below the two

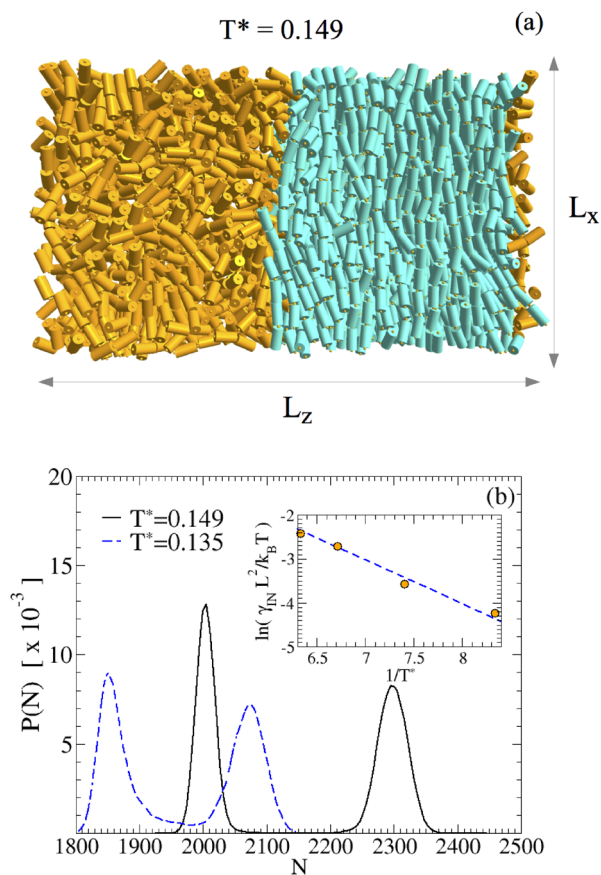


**Figure 2.** (a) Snapshot of a system containing  $N = 2150$  particles at coexistence ( $T^* = 0.149$ ). Orange particles, which are mostly on the left side of the box, are isotropic, while cyan particles on the right side of the box are nematic. (b) Probability distribution  $P(N)$  at coexistence, where  $N$  is the number of HCs in the simulation box, with  $\sum_N P(N) = 1$ , obtained from SUS simulations at  $T^* = 0.135$  and  $0.149$  (box sizes are  $L_x = 13L$ ,  $L_y = 4L$ , and  $L_z = 23.5L$ ). The inset shows the surface tension  $\gamma_{IN}$  calculated from the SUS simulations together with a blue dashed line with a slope of  $-1$ .

peaks. The average value of  $N$  for each of the two peaks provides the value of the volume fractions at coexistence. Because of the elongated shape of the box, the isotropic–nematic interface is stable and forms parallel to the  $xy$  plane, as shown in Figure 2a.

When a clean interface establishes in the simulation box, the depth  $\Delta F$  of the well between the two peaks provides information on the surface tension  $\gamma_{IN}$ , via the relation  $\Delta F = 2\gamma_{IN}L_xL_y$ . Although in our simulations we do not have a clear flat region between the two peaks,  $\Delta F$  provides a rough estimate of the surface tension and it is interesting to note that, as shown in the inset of Figure 2b,  $\gamma_{IN}k_B T$  appears to decrease upon decreasing  $T$  as  $e^{-\beta u_0}$ .

For configurations with nematic order, we checked that no translational order builds up in the system by calculating the three-dimensional pair distribution function  $g(\mathbf{r})$  defined as

$$g(\mathbf{r}) = \frac{1}{\rho N} \left\langle \sum_{i=1}^N \sum_{j \neq i}^N \delta(\mathbf{r} - (\mathbf{r}_i - \mathbf{r}_j)) \right\rangle \quad (2)$$

where  $\delta(\mathbf{x})$  is the Dirac delta function. If the nematic director defines the  $z$  axis,  $g(x, y, 0)$  and  $g(0, y, z)$  correspond respectively to the correlations in a plane perpendicular to the

nematic director and in a plane containing it. Figure 3 shows both  $g(x, y, 0)$  and  $g(0, y, z)$  for  $T = 0.2$  and  $\phi \approx 0.47$ , the

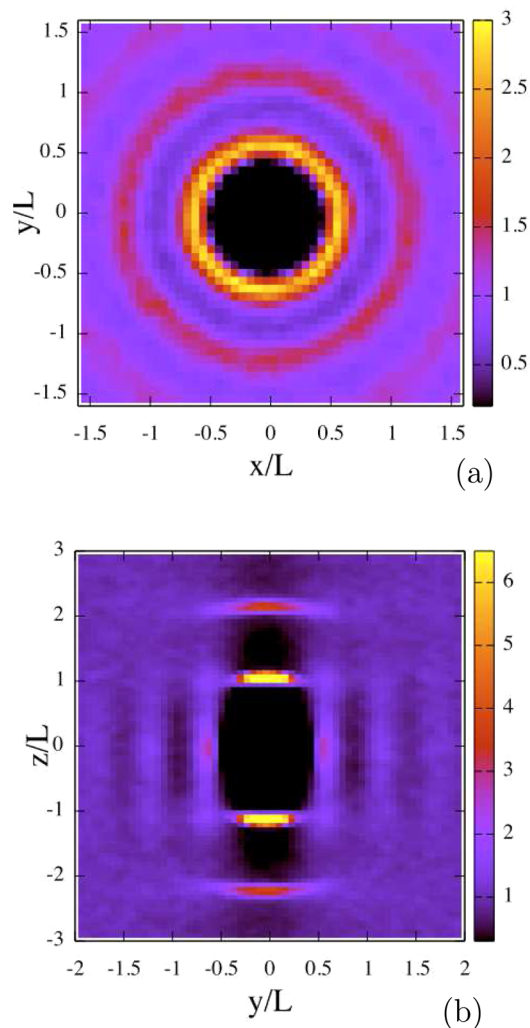


**Figure 3.** Plot of (a)  $g(x, y, 0)$  and (b)  $g(0, y, z)$ , where the  $z$  axis is chosen parallel to the nematic director for  $T^* = 0.2$  and  $\phi = 0.47$ .

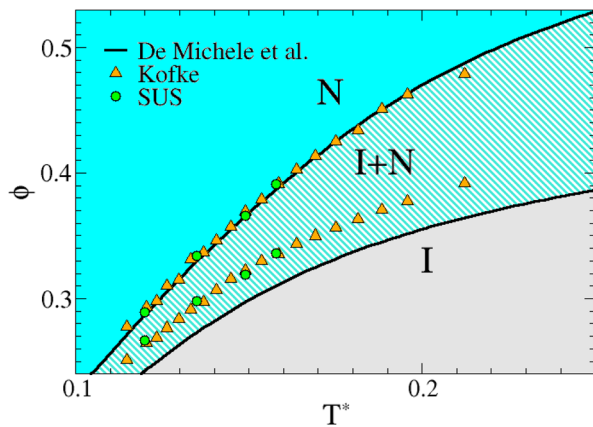
highest investigated volume fraction. These plots, representative of all simulations, show that no columnar, crystal, or smectic phases are observed.

Figure 4 shows the phase boundaries calculated via KI and double checked with independent SUS calculations. The volume fractions of both the isotropic and nematic phases increases upon increasing  $T$ , confirming the expectation that increasing  $T$  disfavors the formation of long aggregates and reduces the driving force for nematization. Panels a and b of Figure 5 show the same numerical data of Figure 4 but in the packing fraction versus average chain aspect ratio,  $X_0 M$ , where  $M$  indicates the average chain length in units of monomers, i.e.

$$M \equiv \frac{\sum_l l \nu(l)}{\sum_l \nu(l)} \quad (3)$$

where  $\nu(l)$  is the number of clusters of size  $l$ .

As shown in Figure 5a, numerical results for the coexisting volume fractions,  $\phi_I$  and  $\phi_N$ , are in good agreement with the predictions made by the theory developed in ref 32 for the present model. Despite the theory slightly underestimating  $M$  in the nematic phase at large  $\phi$ , it captures the re-entrant



**Figure 4.** Isotropic–nematic phase diagram in the packing fraction  $\phi$  versus temperature  $T^*$  plane. Circles are SUS simulations at  $T^* = 0.12, 0.135, 0.149,$  and  $0.158$ . Triangles are results from KI, started from SUS simulation at  $T^* = 0.149$ . The other SUS simulations are used as checkpoints. Lines indicate the theoretical predictions from ref 32.

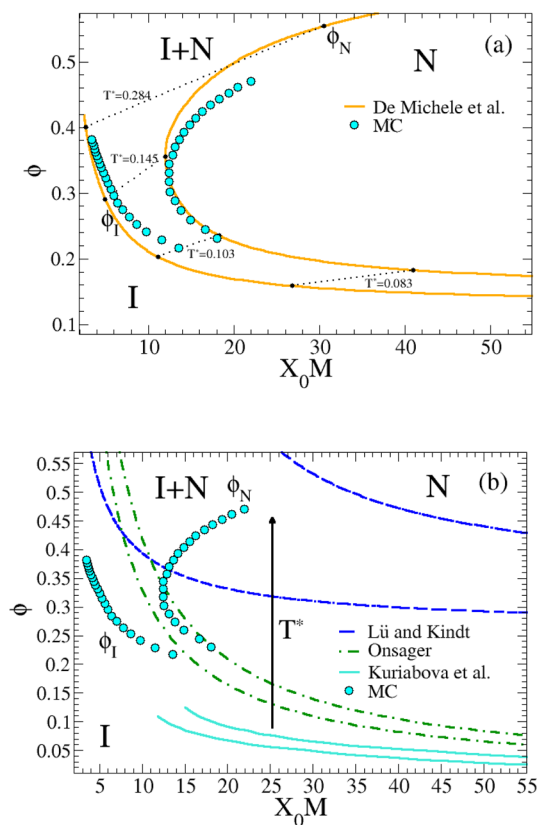


**Figure 5.** Isotropic–nematic coexistence lines in the average aspect ratio  $X_0M$  and volume fraction  $\phi$  plane. In both panels a and b, symbols are numerical results from MC simulations. (a) Solid lines indicate theoretical predictions of ref 32, and full circles along the isotropic and nematic phase boundaries, which are joined by dotted lines, indicate  $\phi$  and  $M$  for isotropic and nematic phases at coexistence at the same temperature. (b) Long-dashed lines are theoretical results from Lü and Kindt's theory,<sup>30</sup> where we set  $k_1 = 37.0, B_1 = 31.8,$  and  $k_N = 36.0$  according to our HC model; dotted-dashed lines indicate the Onsager original predictions, as re-evaluated in ref 54 for  $\phi_I$  and  $\phi_N$ ; and solid lines are theoretical results from ref 31 for  $X_0 = 2.0$ .

behavior. Examining in details the theoretical framework, one notices that such an underestimate in  $M$  arises from the

crudeness of the Parsons–Lee decoupling approximation,<sup>53</sup> entering in the modeling of the excluded volume interactions. If the exponential distribution of chain lengths is approximated with monodisperse cylinders of aspect ratio  $X_0M$ , this representation allows for a comparison to the Onsager theory for HCs, which is shown in Figure 5b. We observe a notable difference between the Onsager predictions and the numerical results. As predicted by Onsager, we find that, upon cooling, the coexistence volume fraction of the isotropic phase  $\phi_I$  decreases, while the average aspect ratio increases, resulting in a monotonic behavior in the  $\phi$ – $X_0M$  plane. Instead, upon cooling, while the coexistence volume fraction of the nematic phases decreases, the average aspect ratio shows a non-monotonic behavior: first decreasing, reaching a minimum value, and then increasing again. Reference 32 allows us to pinpoint the origin of this non-monotonic behavior. The theory indeed shows that the dominant difference between the isotropic and nematic volume fraction dependence of  $M$  is due to an entropic contribution related to the orientational order in the system. This contribution is strongly dependent upon packing and provides an additional burst toward polymerization in the nematic phase at high  $T$ , where nematization takes place at large  $\phi$ .

An argument for grasping the re-entrant behavior can be provided under some simplifying assumptions. If we assume that the cluster size distribution is exponential in both the isotropic and nematic phases and that the chains in the nematic phase are much longer than the persistence length  $l_p$ , then the theoretical framework developed in ref 32 allows us to write in the limiting cases of very high and very low volume fractions

$$\mathcal{R} \equiv \frac{M_N}{M_I} \approx \sqrt{\alpha} \quad (4)$$

where  $M_I$  and  $M_N$  are the average chain length in the isotropic and nematic phases, respectively. The inverse of  $\alpha$  controls the width of the angular distribution of monomer orientations in the nematic phase. When the volume fractions of the nematic phase at coexistence are small (i.e., low temperatures),  $M_N \propto \sqrt{e^{\beta u_0}}$  goes to infinity (see Figure 5 and the Supporting Information). When the volume fractions of the isotropic phase at coexistence are large,  $M_I \approx 1$ . Because the volume fraction of the nematic phase is even larger, we can expect that the angular distribution of the nematic orientation has to be very narrow and, hence, according to the previous equation,  $M_N$  is also very large. From the last two considerations, it follows that  $M_N$  can reasonably exhibit a minimum as a function of  $\phi$ , which is precisely the observed re-entrant behavior shown in Figure 5.

Next, we compare the numerical results to other available theoretical approaches,<sup>30,31</sup> modeling the system as a collection of equilibrium polymers. Different models estimate in different ways the excluded volume interactions between different semi-flexible chains, the role of the bonding free energy, and the orientational entropy (see the Supporting Information for details). Figure 5b shows the results predicted by Lü and Kindt's theory,<sup>30</sup> where the theoretical parameters have been selected to comply with the present hard-cylinder model. Figure 5b shows also the theoretical results from the work of Kuriabova et al.<sup>31</sup> for the HC model studied therein. Similar to the Onsager theory, both of these two approaches do not predict the re-entrant behavior of  $\phi_N$  versus  $X_0M$  discussed previously. In addition, Lü and Kindt's theory largely overestimates the values of  $\phi$  and  $M$  at coexistence.

Finally, because the theoretical approach developed in ref 32 has been derived under two assumptions, namely, that the cluster size distribution is exponential and that monomers are isotropic rather than nematic, we investigate the cluster size distribution along the isotropic and nematic coexistence lines from NPT MC simulations. Figure 6 shows that the

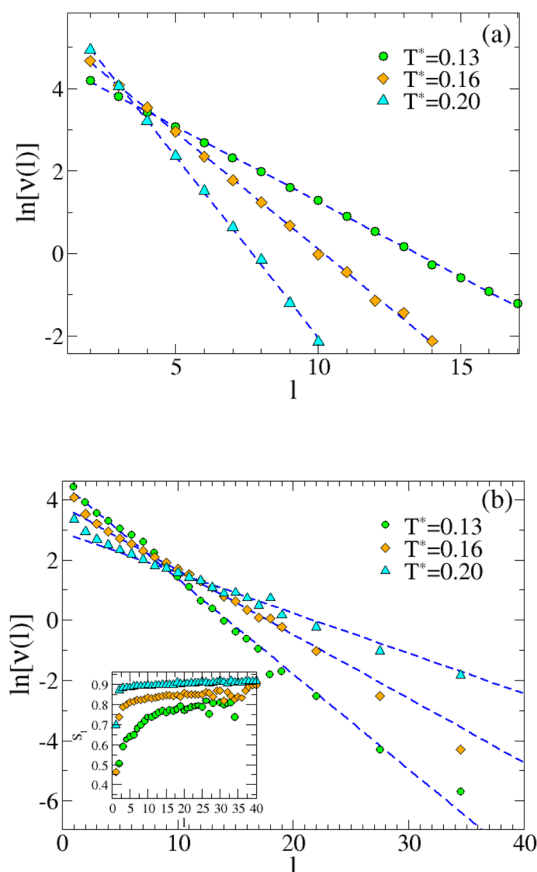


**Figure 6.** Aggregate size distribution  $\nu(l)$  for the (a) isotropic and (b) nematic phases at coexistence, for three different temperatures. Symbols are numerical results, and dashed lines are exponential fits. The inset shows the chain-length-dependent nematic order parameter  $S_1$  for the same state points in the nematic phase.

distribution is a single exponential in the isotropic phase as expected, while in the nematic phase, it can be still described by a single-exponential decay, except for short chains, not to say only monomers at most.

As shown in the inset of Figure 6, the nematic order parameter  $S_1$  for the individual clusters decreases significantly for short chains, providing evidence that, at coexistence, short chains behave differently, retaining an orientational distribution in the nematic phase that is more isotropic (i.e., broader) than the one of longer chains. Here,  $S_1$  has been estimated by evaluating the largest eigenvalue of the order tensor calculated for all monomers belonging to clusters of size  $l$ .<sup>31,55</sup>

We observe that, as discussed in Appendix B of ref 56, finite size effects in the calculation of  $S_1$  are not expected if either (i)  $S_1 > 0.4$ – $0.5$  or (ii) the number of monomers, over which the order tensor is calculated, is larger than  $\approx 10$ . In our simulations,  $S_1$  is always greater than  $0.4$  and the number of considered monomers is always much greater than  $10$ . Hence, both conditions (i) and (ii) are matched in our case.

## CONCLUSION

In conclusion, we determined, through a combined SUS and KI approach, the phase diagram of self-assembling cylinder in the  $\phi$  versus  $T$  plane, the simplest model for describing self-assembly-driven nematization. We observe the re-entrant behavior of the nematic volume fraction along coexistence in the  $\phi$ – $M$  plane, which has been theoretically predicted in ref 32. Our results provide an accurate benchmark for the recent theoretical studies, pointing out the importance of properly modeling excluded volume and orientational entropy. They also provide a reference system for the interpretation of a large class of biologically relevant aggregation processes in the dense limit.<sup>7,11,17</sup> The non-monotonic (re-entrant) behavior of  $M$  along the nematic boundary  $\phi_N$  can be accessed via small-angle static scattering or via measurements of the elastic constants, which are strongly coupled to  $M$ .<sup>16</sup>

## ASSOCIATED CONTENT

### Supporting Information

Details on theoretical and simulation methods that have been used to build the phase diagram, description of numerical methods used to estimate the parameters required by theory, more information on the algorithm that we used to check the overlap between cylinders, and further discussion on the absence of re-entrant behavior in the Kuriabova theory (see ref 31). This material is available free of charge via the Internet at <http://pubs.acs.org>.

## AUTHOR INFORMATION

### Corresponding Author

\*E-mail: [cristiano.demichele@roma1.infn.it](mailto:cristiano.demichele@roma1.infn.it)

### Notes

The authors declare no competing financial interest.

## ACKNOWLEDGMENTS

We acknowledge support from ERC-226207-PATCHYCOLLOIDS and MIUR-PRIN.

## REFERENCES

- (1) Hamley, I. *Introduction to Soft Matter*; John Wiley and Sons: Hoboken, NJ, 2007.
- (2) Glotzer, S. C. Some assembly required. *Science* **2004**, *306*, 419–420.
- (3) Whitesides, G. M.; Boncheva, M. Beyond molecules: Self-assembly of mesoscopic and macroscopic components. *Proc. Natl. Acad. Sci. U. S. A.* **2002**, *99*, 4769–4774.
- (4) Khan, A. Phase science of surfactants. *Curr. Opin. Colloid Interface Sci.* **1996**, *1*, 614.
- (5) van der Schoot, P.; Cates, M. Growth, static light scattering, and spontaneous ordering of rodlike micelles. *Langmuir* **1994**, *10*, 670–679.
- (6) Kuntz, D. M.; Walker, L. M. Nematic phases observed in amphiphilic polyelectrolyte–surfactant aggregate solutions. *Soft Matter* **2008**, *4*, 286–293.
- (7) Mezzenga, R.; Jung, J.-M.; Adamcik, J. Effects of charge double layer and colloidal aggregation on the isotropic–nematic transition of protein fibers in water. *Langmuir* **2010**, *26*, 10401–10405.
- (8) Lee, C. F. Isotropic–nematic phase transition in amyloid fibrilization. *Phys. Rev. E: Stat., Nonlinear, Soft Matter Phys.* **2009**, *80*, 031902.
- (9) Ciferri, A. On collagen II fibrillogenesis. *Liq. Cryst.* **2007**, *34*, 693–696.
- (10) Aggeli, A.; Bell, M.; Carrick, L. M.; Fishwick, C. W. G.; Harding, R.; Mawer, P. J.; Radford, S. E.; Strong, A. E.; Boden, N. pH as a

trigger of peptide  $\beta$ -sheet self-assembly and reversible switching between nematic and isotropic phases. *J. Am. Chem. Soc.* **2003**, *125*, 9619–9628.

(11) Nakata, M.; Zanchetta, G.; Chapman, B. D.; Jones, C. D.; Cross, J. O.; Pindak, R.; Bellini, T.; Clark, N. A. End-to-end stacking and liquid crystal condensation of 6 to 20 base pair DNA duplexes. *Science* **2007**, *318*, 1276.

(12) Maffeo, C.; Luan, B.; Aksimentiev, A. End-to-end attraction of duplex DNA. *Nucleic Acids Res.* **2012**, *40*, 3812–3821.

(13) Robinson, C. Liquid-crystalline structures in polypeptide solutions. *Tetrahedron* **1961**, *13*, 219–234.

(14) Livolant, F.; Levelut, A. M.; Doucet, J.; Benoit, J. P. The highly concentrated liquid-crystalline phase of DNA is columnar hexagonal. *Nature* **1989**, *339*, 724–726.

(15) Merchant, K.; Rill, R. L. DNA length and concentration dependencies of anisotropic phase transitions of DNA solutions. *Biophys. J.* **1997**, *73*, 3154–3163.

(16) Tombolato, F.; Ferrarini, A. From the double-stranded helix to the chiral nematic phase of B-DNA: A molecular model. *J. Chem. Phys.* **2005**, *122*, 054908.

(17) Mariani, P.; Spinozzi, F.; Federiconi, F.; Amenitsch, H.; Spindler, L.; Drevensek-Olenik, I. Small angle X-ray scattering analysis of deoxyguanosine 5-monophosphate self-assembling in solution: Nucleation and growth of G-quadruplexes. *J. Phys. Chem. B* **2009**, *113*, 7934–7944.

(18) Chami, F.; Wilson, M. R. Molecular order in a chromonic liquid crystal: A molecular simulation study of the anionic azo dye sunset yellow. *J. Am. Chem. Soc.* **2010**, *132*, 7794–7802.

(19) Lydon, J. Chromonic liquid crystalline phases. *Liq. Cryst.* **2011**, *38*, 1663–1681.

(20) Maiti, P. K.; Lansac, Y.; Glaser, M. A.; Clark, N. A. Isodesmic self-assembly in lyotropic chromonic systems. *Liq. Cryst.* **2002**, *29*, 619–626.

(21) Edwards, R. G.; Henderson, J.; Pinning, R. L. Simulation of self-assembly and lyotropic liquid crystal phases in model discotic solutions. *Mol. Phys.* **1995**, *86*, 567–598.

(22) Henderson, J. R. Discotic amphiphiles. *J. Chem. Phys.* **2000**, *113*, 5965–5970.

(23) Liu, K.; Nie, Z.; Zhao, N.; Li, W.; Rubinstein, M.; Kumacheva, E. Step-growth polymerization of inorganic nanoparticles. *Science* **2010**, *329*, 197–200.

(24) Taylor, M. P.; Herzfeld, J. Liquid-crystal phases of self-assembled molecular aggregates. *J. Phys.: Condens. Matter* **1993**, *5*, 2651.

(25) Sciortino, F.; Douglas, J.; De Michele, C. Growth of equilibrium polymers under non-equilibrium conditions. *J. Phys.: Condens. Matter* **2008**, *20*, 155101.

(26) Park, H.-S.; Kang, S.-W.; Tortora, L.; Nastishin, Y.; Finotello, D.; Kumar, S.; Lavrentovich, O. D. Self-assembly of lyotropic chromonic liquid crystal sunset yellow and effects of ionic additives. *J. Phys. Chem. B* **2008**, *112*, 16307–16319.

(27) Wilding, N. B. Simulation studies of fluid critical behaviour. *J. Phys.: Condens. Matter* **1996**, *9*, 585–612.

(28) Onsager, L. The effects of shape on the interaction of colloidal particles. *Ann. N. Y. Acad. Sci.* **1949**, *627*.

(29) Herzfeld, J. Entropically driven order in crowded solutions: From liquid crystals to cell biology. *Acc. Chem. Res.* **1996**, *29*, 31–37.

(30) Lü, X.; Kindt, J. Monte Carlo simulation of the self-assembly and phase behavior of semiflexible equilibrium polymers. *J. Chem. Phys.* **2004**, *120*, 10328–10338.

(31) Kouriabova, T.; Betterton, M.; Glaser, M. Linear aggregation and liquid-crystalline order: Comparison of Monte Carlo simulation and analytic theory. *J. Mater. Chem.* **2010**, *20*, 10366–10383.

(32) De Michele, C.; Bellini, T.; Sciortino, F. Self-assembly of bifunctional patchy particles with anisotropic shape into polymers chains: Theory, simulations, and experiments. *Macromolecules* **2012**, *45*, 1090–1106.

(33) McGrother, S. C.; Williamson, D. C.; Jackson, G. A re-examination of the phase diagram of hard spherocylinders. *J. Chem. Phys.* **1996**, *104*, 6755.

(34) Frenkel, D.; Mulder, B. M. The hard ellipsoid-of-revolution fluid I. Monte Carlo simulations. *Mol. Phys.* **1991**, *55*, 1171–1192.

(35) Dijkstra, M.; Frenkel, D. Simulation study of the isotropic-to-nematic transitions of semiflexible polymers. *Phys. Rev. E: Stat. Phys., Plasmas, Fluids, Relat. Interdiscip. Top.* **1995**, *51*, 5891–5898.

(36) Dennison, M.; Dijkstra, M.; van Roij, R. Phase diagram and effective shape of semiflexible colloidal rods and biopolymers. *Phys. Rev. Lett.* **2011**, *106*, 208302.

(37) Camp, P. J.; Mason, C. P.; Allen, M. P.; Khare, A. A.; Kofke, D. A. The isotropic–nematic phase transition in uniaxial hard ellipsoid fluids: Coexistence data and the approach to the Onsager limit. *J. Chem. Phys.* **1996**, *105*, 2837–2849.

(38) Wensink, H.; Lekkerkerker, H. Phase diagram of hard colloidal platelets: A theoretical account. *Mol. Phys.* **2009**, *107*, 2111–2118.

(39) Gámez, F.; Merkling, P.; Lago, S. Parsons–Lee approach for oblate hard spherocylinders. *Chem. Phys. Lett.* **2010**, *494*, 45–49.

(40) Dogic, Z.; Fraden, S. Ordered phases of filamentous viruses. *Curr. Opin. Colloid Interface Sci.* **2006**, *11*, 47–55.

(41) Padmanabhan, V.; Kumar, S. K.; Yethiraj, A. Phase behavior of semiflexible polymer chains. *J. Chem. Phys.* **2008**, *128*, 124908.

(42) Jiang, T.; Wu, J. Isotropic–nematic phase transition in athermal solutions of rod–coil diblock copolymers. *J. Chem. Phys.* **2007**, *127*, 034902.

(43) Tkachenko, A. Isotropic–nematic–smectic: Importance of being flexible. *Phys. A* **1998**, *249*, 380–385.

(44) De Michele, C.; Rovigatti, L.; Sciortino, F. Self-assembly of short DNA duplexes: From a coarse-grained model to experiments through a theoretical link. *Soft Matter* **2012**, *8*, 8388.

(45) Henderson, J. R. Concentration dependence of linear self-assembly and exactly solvable models concentration dependence of linear self-assembly and exactly solvable models. *Phys. Rev. Lett.* **1996**, *77*, 2316–2319.

(46) Henderson, J. R. Physics of isodesmic chemical equilibria in solution. *Phys. Rev. E: Stat. Phys., Plasmas, Fluids, Relat. Interdiscip. Top.* **1997**, *55*, 5731–5742.

(47) Vega, C.; Sanz, E.; Abascal, J. L. F.; Noya, E. G. Determination of phase diagrams via computer simulation: Methodology and applications to water, electrolytes and proteins. *J. Phys.: Condens. Matter* **2008**, *20*, 153101.

(48) Kofke, D. A. Direct evaluation of phase coexistence by molecular simulation via integration along the saturation line. *J. Chem. Phys.* **1993**, *98*, 4149–4162.

(49) Tian, P.; Bedrov, D.; Smith, G. D.; Glaser, M. A molecular dynamics simulation study of the phase behavior of an ensemble of rigid bead-necklace molecules. *J. Chem. Phys.* **2001**, *115*, 9055–9064.

(50) Almaraz, N. G. A cluster algorithm for Monte Carlo simulation at constant pressure. *J. Chem. Phys.* **2009**, *130*, 184106.

(51) Virnau, P.; Müller, M. Calculation of free energy through successive umbrella sampling. *J. Chem. Phys.* **2004**, *120*, 10925–10930.

(52) Vink, R. L. C.; Schilling, T. Interfacial tension of the isotropic–nematic interface in suspensions of soft spherocylinders. *Phys. Rev. E: Stat., Nonlinear, Soft Matter Phys.* **2005**, *71*, 051716.

(53) Parsons, J. D. Nematic ordering in a system of rods. *Phys. Rev. A: At., Mol., Opt. Phys.* **1979**, *19*, 1225–1230.

(54) Vroege, G. J.; Lekkerkerker, H. N. W. Phase transitions in lyotropic colloidal and polymer liquid crystals. *Rep. Prog. Phys.* **1992**, *55*, 1241–1309.

(55) Eppenga, R.; Frenkel, D. Monte Carlo study of the isotropic and nematic phases of infinitely thin hard platelets. *Mol. Phys.* **1984**, *52*, 1303–1334.

(56) Richter, A.; Gruhn, T. Structure formation and fractionation in systems of polydisperse attractive rods. *J. Chem. Phys.* **2006**, *125*, 64908.